ACS OMEGA

http://pubs.acs.org/journal/acsodf

Article

Diamond-like Carbon Patterning by the Submerged Discharge Plasma Technique via Soft Solution Processing

Sumanta Kumar Sahoo, Ravi Bolagam, Kripasindhu Sardar, Satoru Kaneko, Shih-Chen Shi, Kao-Shuo Chang, and Masahiro Yoshimura*

Cite This: *ACS Omega* 2023, 8, 17053−17063

Read Online

ACCESS | Metrics & More | Article Recommendations | Supporting Information

ABSTRACT: Submerged plasma-assisted discharge direct patterning of diamond-like carbon (DLC) onto the silicon substrate in ambient conditions has succeeded as a new and novel soft solution process. In this environmentally benign technique, a copious amount of pure ethanol (ca. 4 mL) was locally activated with a maximum of ca. 0.23 mkWh by an as-electrochemically synthesized ultrasharp tungsten tip. With the assisted submerged plasma, the decomposed ethanol molecules are anodically patterned directly onto the silicon substrate in ambient conditions. The physical nature of DLC patterns was accessed by profilometry, atomic force microscopy, scanning electron microscopy, and transmission electron microscopy analysis. Furthermore, Fourier-transform infrared, Raman, and X-ray photoelectron spectra were analyzed for chemical compositions and structures, such as surface functionalization, carbon−carbon bonding, and sp^2−sp^3 ratio, respectively. From a Berkovich-configured nanoindentation analysis, Young's modulus and hardness have shown increasing trend with increasing sp^3−sp^2 ratio in DLC patterns of 68.5 and 2.8 GPa, respectively. From the electrochemical cyclovoltammetry analysis, a maximum areal specific capacitance of 205.5 $\mu F/cm^2$ has been achieved at a scan rate of 5 mV/s. The one-step, green, and environmentally sustainable approach of rapid formation of DLC patterns is thus a promising technique for various carbon-based electrode fabrication processes.

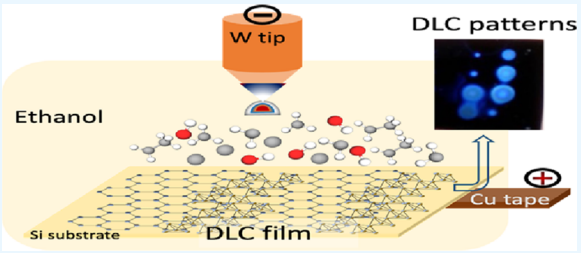

1. INTRODUCTION

Diamond-like carbon (DLC) is well known to outperform amorphous carbon material composed of the sp^3- and sp^2-hybridized carbon phase along with hydrogen atoms.[1,2] It is well known for low friction, high wear resistance, high thermal stability, chemical inertness, and high electrical resistivity due to the presence of higher sp^3 (diamond phase) in the amorphous carbon matrix.[3,4] Its intriguing properties such as high Young's modulus, wide bandgap, high carrier mobility, low thermal expansion coefficient, and biocompatibility nature of the DLC materials give a unique platform for various technological advancements. Due to its robustness in material properties, it has been applied in a wide range of technological applications such as microelectromechanical systems, protective coatings, field emission, field-effect transistor, and bio-applications.[5−7]

The interest in DLC films started nearly four decades ago, and a significant leap has been observed from the laboratory to the industry till date. Typically, DLC has been classified into four types such as amorphous carbon (a-C), hydrogenated amorphous carbon (a-C:H), tetrahedral amorphous carbon (ta-C), and hydrogenated tetrahedral amorphous carbon (ta-C:H) based on their relative sp^3 carbon and hydrogen content. Hydrogenated DLCs are formed by various hydrocarbon sources, whereas the hydrogen-free DLCs have mostly used a solid carbon ion beam in a vacuum system. The pioneer work of Aisenberg and Chabot[8] in using a carbon cation beam to deposit onto the cathode substrate in a low pressure vacuum chamber was the first report in the DLC deposition technique. After that, there is the introduction of the hydrocarbon source in the deposition chamber to increase the deposition rate, which essentially exhibits hydrogenated DLC. Physical vapor deposition (PVD) by the ion beam of carbon in vacuum conditions essentially produces a high quality non-hydrogenous DLC film.[9,10] Chemical vapor deposition (CVD) uses various carbon sources such as methane (CH_4), ethylene (C_2H_2), cyclohexane (C_6H_{12}), etc., which are activated by plasma, radio frequency, and dc glow discharge process techniques for preparing hydrogenated DLC films.[11,12] Again, various carbonaceous materials including DLCs can also be synthesized by catalyst-assisted thermal reduction of CO_2 under relatively high temperature and pressure conditions.[13−15]

Received: February 27, 2023
Accepted: April 19, 2023
Published: May 4, 2023

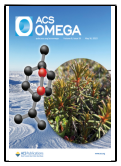

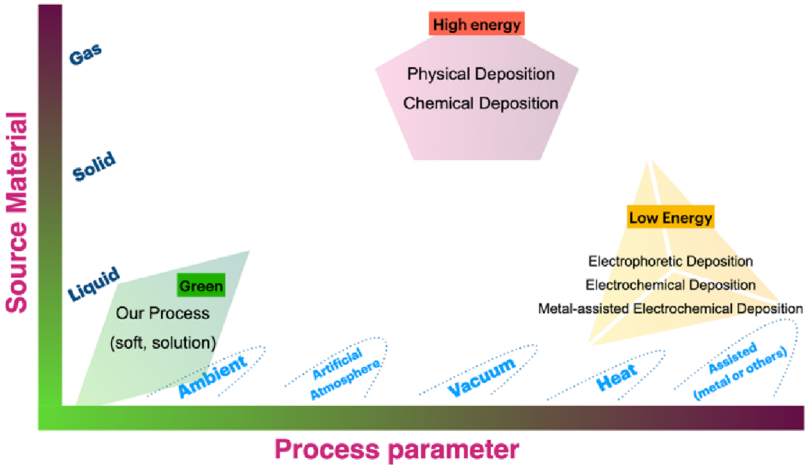

Figure 1. Overview process parameters of various DLC patterning in comparison to the present reported (soft solution) process mechanism.

Though these techniques provide a uniform and well-controlled sp^2-sp^3 phase in the DLC coating, however, slower deposition rate and complex process controlling parameters such as substrate temperature, catalysts, and gas mixture limit sustainable production.

The PVD technique uses a solid carbon target to vaporize into carbon ions in vacuum conditions and their subsequent deposition onto the substrate. These techniques used high energetic beams such as plasma and laser source in an artificial environment. Similarly, the CVD technique also includes different organic carbon phases in gaseous form and is activated (by radiofrequency and plasma) to deposit onto a substrate.[16] In general, PVD and CVD processes use multi-step processing such as cleaning, masking, etching, annealing, etc., for a high-quality DLC film. However, these advanced techniques come with few limitations, such as the scale-up to the industrial level, complex controlling parameters, release of toxic gases to the atmosphere, and slow development in DLC film formation. Another category uses electrochemical force to deposit DLC on a conductive substrate from various organic solvents. The pioneering work of Namba[17] has initiated this low-energy process of electrochemical deposition from ethanol onto the silicon substrate at a solution temperature of up to 60−70 °C. After that, various organic solvents such as methanol, *N*,*N*-dimethylformamide (DMF), acetonitrile, nitromethane, nitroethane, ethylene glycol, and dimethyl sulfoxide have been experimented for electrochemical DLC formation.[18−21] However, these electrochemical deposition processes required a very high-power supply to decompose the organic electrolyte before deposition, required maintenance of heat to the whole electrolyte system, or performed at a slower rate of deposition. Novikov and Dymont[22] proposed that the electrochemical deposition of DLC can be carried out at 20−100 °C of electrolyte temperature with the addition of transition metal salt into the electrolyte. In summary, the DLC deposition process was basically carried out by PVD, CVD, and electrochemical process in solution with the aid of high activation energies. On the other hand, Yoshimura, one of the co-authors, has proposed soft processing or soft solution processing since the late 90s. This was derived from "soft chemistry" (chimie douce), which aim soft, environmentally friendly fabrication of materials. Thus, not only synthesis but also shape/size/location/orientation-controlled materials like films and patterns,[23−25] particularly "direct patterning" of inorganic materials in and/or from solution or liquid, have not been well studied yet. Therefore, here we have been interested not only in DLC deposition but also in one-step direct patterning to fabricate DLCs from solution.[26]

In the present study, we have proposed a green, sustainable, and novel strategy for DLC patterning by plasma-assisted discharge in the submerged state. This is the first ever report in detailed analysis about the patterning of the DLC film by using the lowest activation energy onto the silicon substrate by the electrochemical-assisted microplasma-based approach in submerged conditions. With a copious amount of pure ethanol solvent and fast fabrication process under ambient conditions, the proposed soft solution process shows very simple, efficient, and robust processing for DLC fabrication. Young's modulus, hardness, and electrochemical charge storage properties were assessed along with other physiochemical studies of the patterned DLC.

2. PROPOSAL STRATEGY FOR DIRECT PATTERNING

In most of the previous studies, patterning of inorganic materials has been done via (i) multi-step processing after film formation from solid particles and/or gaseous precursors like vapors (CVD) or atoms/ions (PVD) and then making patterns like lithography via masking/etching or (ii) ion beam/atomic beam direct writing via highly energetic species. They have generally consumed lots of energy and then exhaust lots of wastes (materials and energy); thus, the process is neither soft nor green. Therefore, in this report, we would like to propose "direct patterning" of inorganic materials in a liquid and/or solution under ambient pressure and temperature conditions. As it can be seen from Figure 1, we have used DLC film formation with submerged plasma in liquid with a needle-like electrode. The automated *x*-*y*-*z* motions could enable us to draw 1D and 2D patterns onto the counter electrode. This direct patterning of DLC has the following merits; (i) it is essentially a single step, not a multi-step (particle synthesis, dispersion in a liquid (ink), printing, firing, etc.), (ii) it can be performed in a liquid under ambient conditions, (iii) the liquid can be recovered and is recyclable, and (iv) various liquids may be used even as mixed ones for various materials and/or various micro/nanostructures. Of course, the control of electro plasma discharge is not easy but controllable. Anyway, this "direct patterning strategy" should be soft and green compared to any other method.

https://doi.org/10.1021/acsomega.3c01322
ACS Omega 2023, 8, 17053−17063

3. EXPERIMENTAL SECTION

3.1. Materials. All the chemicals used were of analytical grade and were used without further purification. A high pure assay of (>99.9%) ethanol reagent was purchased from J.T. Baker. A high pure (99.95%) tungsten (W) wire of 0.1 mm diameter was purchased from Ultimate Materials Technology Co., Ltd., Taiwan. The silicon substrate of N-type Si(100) with a resistivity of 1−10 Ω cm was used. A low power dc supply from AVTECH (Model: AV-1022-C) was used in the W-tip fabrication process, and a high voltage dc power supply from Matsusada Precision Inc. (Model: AU-40P 1.5) was used for the patterning experiments. For patterning, a highly precision controlled three-axial compact motorized actuator CONEX−TRA25CC, NEWPORT was used for automatic motion control with a LabView program.

3.2. Characterization. As-synthesized DLC patterns subjected to various structural, morphological, topographical, chemical bonding, and functional group analysis were performed by using high precision and calibrated scientific equipment. The thickness measurement of the DLC film was performed by a profilometer of KLA-Tencor, AS-IQ, Alpha-Step D-300 model. The stylus is a diamond tip of a radius of 2 μm, and a scanning speed of 50 μm/s was used with an applied stylus force of 2 mg. The topological information was collected from atomic force microscopy (AFM) of model XE7, Park Systems, and the images were processed by XEI software. The morphological analysis was carried out by JEOL, JSM-6701F field-emission scanning electron microscopy (FESEM), and JEOL, JEM-2100F CS STEM transmission electron microscopy (TEM). Fourier transform infrared (FTIR) spectroscopy studies were performed using JASCO, FT/IR-4600 model, with a scanning range from 4000 to 700 cm^{-1} in transmittance mode. The Raman spectra were recorded by using a 532 nm excitation wavelength from MRI, Protrustech Co., Ltd. X-ray photoelectron spectroscopy (XPS) measurements were performed by PHI Hybrid Quantera with monochromatic Al Kα (E = 1.487 keV) X-ray radiation. Data analysis was performed using XPSPEAK41 software. The nanoindentation measurements were performed using a Hysitron TI 950 triboindenter, Bruker.

3.3. Electrochemical Analysis. The three-electrode configured electrochemical setup was used for measuring the electrochemical performance of the DLC pattern electrodes in the 0.5 M Na_2SO_4 electrolyte using a Multi AUTOLAB M204 (serial no. MAC90422) electrochemical workstation. The as-prepared electrode, platinum plate, and Ag/AgCl electrode were used as the working electrode, the counter electrode, and the reference electrode, respectively. The electrochemical tests included cyclic voltammetry (CV) under different scan rates (5−100 mV/s) in a −0.8 to 0 V potential window and electrochemical impedance spectroscopy (EIS) in the frequency range of 0.01 Hz to 100 kHz with an AC perturbation of 5 mV. The areal specific capacitance (C_{sp}) of the electrodes was precisely determined through CV curves by the formula

$$C_{sp} = \frac{\int I dV}{2 \times V \times \nu \times A} \quad (1)$$

where I is the current, V is the voltage window, ν is the scan rate, and A is the area of active material.

3.4. Patterning of DLC. A configured ultrasharp tungsten (W) tip was prepared by the conventional electrochemical etching process in an aqueous KOH electrolyte. The cell configurations, process parameters, and mechanism of W-tip evolution are described in the Supporting Information, Section S1 with schematic representation, as shown in Figure S1. The as-synthesized W-tip profile (as shown in Figure S2) consists of a radius of curvature (RoC) of 3 μm with a tapper angle (θ) of 12°. The W-tip was used to generate continuous plasma at the tip of the surface along the interface with the solvent and silicon substrate. The mathematical approximation (see the Supporting Information, Section S3) depicts at a dc bias of 1.5 kV with 1 mA current, and the W-tip surface profile induces a plasmonic temperature of ca. 5370 K at a very high current density of 1.7×10^7 A/m^2. Three different carbon coatings on the silicon surface were performed by applying 0.5, 1.0, and 1.5 kV dc bias to the W-tip for 10 min each by maintaining an emission current of 1 mA from the as-prepared W-tip. The W-tip was used as a microplasma probe to generate a sp^2−sp^3 hybrid mixture of carbon nanostructures from a pure ethanol solvent. The uniqueness of the patterning of the carbon thin films on the silicon substrate by the microplasma process was ascribed here.

4. RESULTS AND DISCUSSION

4.1. Formation and Fabrication of the DLC Pattern. The microplasma-based electrochemically decomposed ethanol molecules generated various highly energetic carbon radicals and ions. Due to the extreme amount of heat generation at the sharp W-tip, the decomposed carbon radicals have gained high kinetics and randomly bombarded on the anodized silicon surface. The carbon particles are chemically bonded with each other to form thin films of carbon nanostructures. Similar works called solution plasma methods have been reported by Saito et al.,[27,28] and they also reported similar high-energy species in solution. They reported nanoparticles[27] and polymerized films[28] but not the direct shape forming patterning of materials. A typical carbon patterning at various deposition conditions onto the silicon surface is shown in Figure 2a. This is the confirmation of one of the previous works on carbon patterning.[26] Here onward,

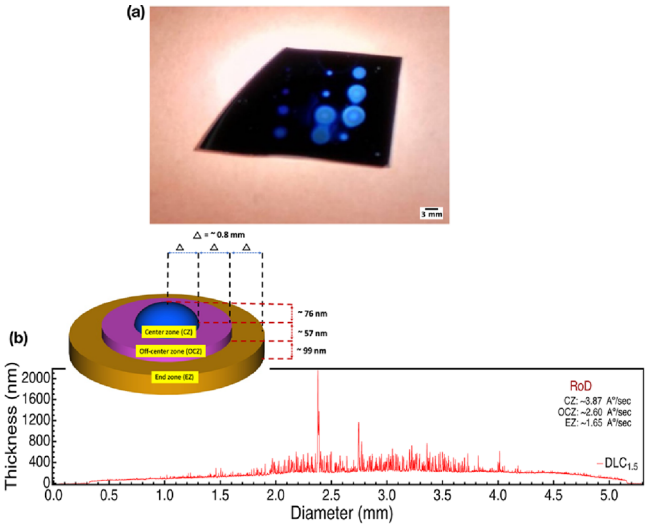

Figure 2. Typical DLC patterns onto the silicon substrate under various deposition conditions (a) and surface profilometer scan of $DLC_{1.5}$ (b) (inset: patterned surface profile schematics with thickness parameters).

https://doi.org/10.1021/acsomega.3c01322
ACS Omega 2023, 8, 17053−17063

the carbon patterned film synthesized by the plasma-based electrochemical approach is now named as diamond-like carbon (DLC) patterning. $DLC_{0.5}$, $DLC_{1.0}$, and $DLC_{1.5}$ represent the carbon film deposited by microplasma-based electrochemical decomposition of ethanol at applied dc biases of 0.5, 1.0, and 1.5 kV, respectively. The physical nature of these thin films has been studied using a surface profilometer. It has been observed that the circular carbon patterns were a few millimeters in diameter. The diameter of the carbon thin film for $DLC_{1.5}$ was ca. 4.82 mm, as shown in the profilometry analysis from Figure 2b. Again, the diameters of carbon thin films were 3.95 and 4.27 mm for $DLC_{0.5}$, and $DLC_{1.0}$, respectively, as calculated from the profilometry data analysis, as shown in the Supporting Information, Figure S3. Each circular pattern was equally sectioned into three annular parts from the center of the circle, as shown in the inset of Figure 2b. A taper-type growth of the carbon structures was observed, where the central, off-center, and end zone consist of thicker particulates and smoother and ultrasmoother surfaces in the carbon surfaces, respectively. The central portion is poised with a highly rough surface, which may attribute directly beneath the W-tip, where large carbon particulates bombard onto the silicon surface. Different rates of deposition (RoD) of carbon nanostructures at various zones in the circular carbon pattern structures were observed. From the thickness profilometry data analysis, the RoDs were maximum at the center compared to the other zones of patterned films. The average RoDs at the center zone of the carbon nanostructures are 2.72, 3.23, and 3.87 Å/s for $DLC_{0.5}$, $DLC_{1.0}$, and $DLC_{1.5}$ films, respectively. The thickness profile and the RoD at various zones were measured and calculated for all the DLC films, as shown in Table 1. Hereafter, all the analyses performed are taken from the off-center zone of the DLC films due to the compactness in the surface structure.

Table 1. Surface Profilometry Data Analysis of DLC Films and RoD Parameters

	rate of deposition (RoD) (in Å/s)		
type of DLC film	center zone(CZ)	off-center zone(OCZ)	end zone(EZ)
$DLC_{0.5}$	2.72	1.93	0.95
$DLC_{1.0}$	3.23	2.05	1.28
$DLC_{1.5}$	3.87	2.60	1.65

4.2. Microscopic Analysis. The three-dimensional (3D) AFM image analysis of the carbon thin film, as shown in Figure 3a, depicts a smooth surface roughness of 14.4 nm at 1.5 kV applied dc bias. In contrast, the surface roughnesses of the carbon film deposited at 0.5 and 1.0 kV show high roughness values of 44.5 and 15.4 nm, respectively. This fact may be attributed to the optimum growth rate of the carbon-nucleated nanostructure at 1.5 kV, whereas at 0.5 and 1.0 kV, the decomposition as well as the growth of the carbon thin film is under the threshold limit. The 3D AFM image analysis (as shown in the Supporting Information, Figure S4) of the carbon thin film developed at 0.5 and 1.0 kV applied bias depicts the cease at the nucleation and the continual intermediate growing stage of carbon nanostructures on the silicon surface. At 0.5 kV of applied dc bias, the shallow decomposition of the ethanol solvent occurs, and the carbon radicals/particulates form nucleated clusters on the silicon surface, as observed from the AFM image. A higher roughness was observed in the $DLC_{0.5}$ film in contrast to other DLC patterned films that may attribute to low bias and low ROD of carbon molecules. However, at 1.0 kV, there is a significant and uniform growth in the carbon film, leading to a relatively smooth surface that was observed in the DLC film structure.

The SEM image (Figure 3b) of the carbon film obtained at 1.5 kV bias decomposition of ethanol shows uniform grown carbon nanostructures on the silicon substrate. It can be observed that the nucleated carbon particles/radicals coalesced together to form micromushroom-like structures. This coalesced force between the nucleated carbon from the anodized silicon substrate and the evolved carbon radicals from the electrolyte arises from the electromotive force as well as the kinetic throughput from the W-tip apex. These mushroom-like carbon nanostructures were grown uniformly with high decomposition rate of ethanol to form a relatively smooth surface. However, at 0.5 and 1.0 kV applied dc electric fields, the SEM image (as shown in the Supporting Information, Figure S5) of the carbon thin film shows the finer carbon granules and small grains grown on the silicon surface, which in turn depicts the nucleation and intermediate growth stage of carbon films, respectively. The high-resolution TEM image (Figure 3c) reveals the amorphous nature of the as-deposited carbon film on the silicon substrate. The inset of Figure 3c shows the SAED pattern, indicating the amorphous phase of carbon deposits. It is presumed that the carbon deposits from the ethanol source derived by microplasma result in a mixture of sp^3- and sp^2-hybridized carbon thin films.

Furthermore, spectroscopy analysis has been performed to classify the functional nature of the carbon patterned thin films.

4.3. Physicochemical Studies of Patterned DLC. The functional groups as well as the chemical bonding nature of the carbon thin films derived from the plasma-based electrodeposition technique are analyzed by FTIR, Raman, and XPS measurements. Since the deposition process is involved in a high rate decomposition of a pure ethanol solvent by applying a strong electric field onto the anodized silicon substrate, various hydroxylation functional endowments with a mixture of sp^2−sp^3-hybridized bonding in the carbon thin film have been observed.

The decomposition of a pure ethanol solvent and their subsequent deposition onto the anodized silicon substrate at very strong dc bias resulted in the endowment of various hydro-oxygenations in the DLC films. The FTIR spectra as shown in Figure 4 were analyzed for the functional bonding information of the plasma-based thin carbon film deposits. The peaks at ∼2980 and ∼2892 cm^{-1} arise from $-CH_3$- and $-CH_2$-hybridized asymmetric and symmetric C−H stretching, respectively.[29,30] These two peaks were more prominent in the DLC film formed at 0.5 and 1.0 kV, rather than the very weak intense peak by the 1.5 kV DLC film. This fact may be attributed to the nucleation and growth stage of the DLC film, and the carbon molecules were endowed with more hydroxylation functional groups than the fully formed DLC film onto the silicon substrate. The prominent C−H bonding is ascribed to the molecular level of the intermediate growing stage of anions of carbon entity ($C_2H_3^*$, CH_3^*, CH_2^-, etc.) onto the anodized silicon substrate, which may disappear in the DLC film at 1.5 kV due to the oxygenation dominance on the surface. The feebly weaker peak at ∼1620 cm^{-1} in the $DLC_{1.5}$ was ascribed to C═C aromatic stretching of sp^2 carbon rings, which was absent in the intermediate growing stage of DLC films. A strong peak at ∼1043 cm^{-1} in all three types of the

https://doi.org/10.1021/acsomega.3c01322
ACS Omega 2023, 8, 17053−17063

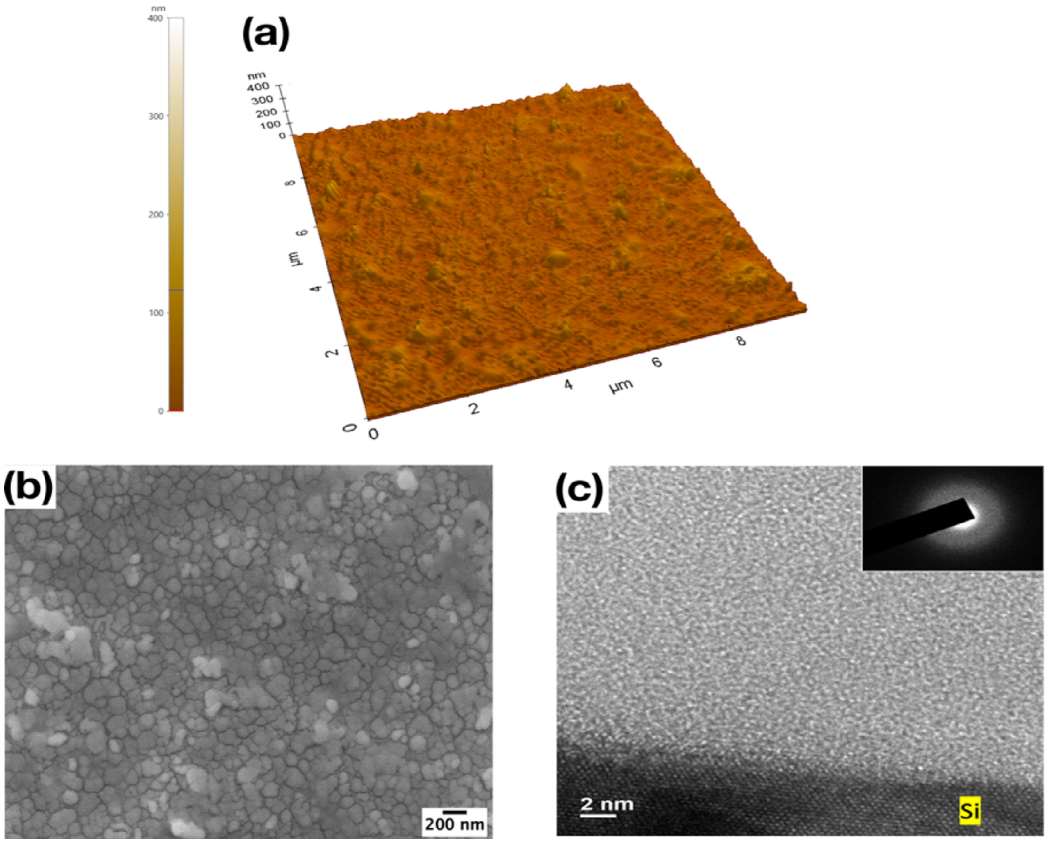

Figure 3. Three-dimensional AFM topography (a), SEM (b), and high-resolution TEM image (c) (inset: SAED pattern) of the $DLC_{1.5}$ pattern.

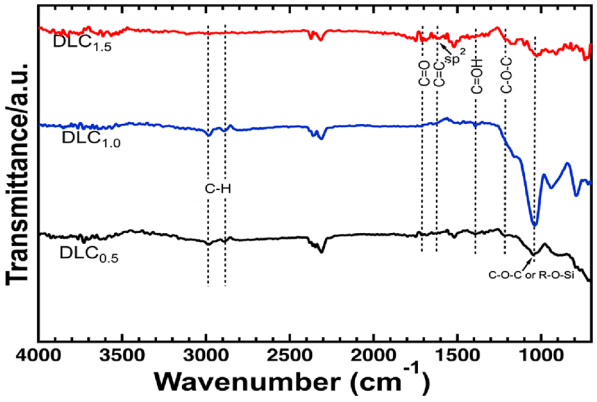

Figure 4. FTIR spectra of $DLC_{0.5}$, $DLC_{1.0}$, and $DLC_{1.5}$ patterns.

DLC film can be assigned to R(alkyl)−O−Si or C−O−C bond stretching as the carbon patterns are anchored to the silicon substrate.[31,32] The DLC film formed at a 1.5 kV applied bias is a fully grown carbon nanostructure and is smoothly interconnected with island-type nucleation followed by growth at relatively lower applied dc biases of 0.5 and 1.0 kV. It is presumed that the stretched-out $DLC_{1.5}$ film on the silicon surface may contribute to a higher/prominent oxygen functional endowment due to reduced hydrogenation functional grain boundaries. This fact can be well observed from the visible intense absorbance IR peaks in the case of $DLC_{1.5}$ in contrast to other DLC structures. The stretching vibrations from various carbo-oxylation functional groups such as carbonyl (C═O), carboxyl (C−OH), and epoxide (C−O−C) are associated with the peaks at ∼1710, ∼1392, and ∼1214 cm^{-1}, respectively.[33,34] From the IR analysis, all the three DLC films showed the composition of sp^2 and sp^3 hybridization of carbon nanostructures with variation in oxygen and hydrogen functionalization contents.

Raman spectral measurements were performed by using an excitation beam of 532 nm from a diode pumped solid-state laser source. The Raman spectral analysis of the as-synthesized DLC films, as observed in Figure 5, shows significant variation

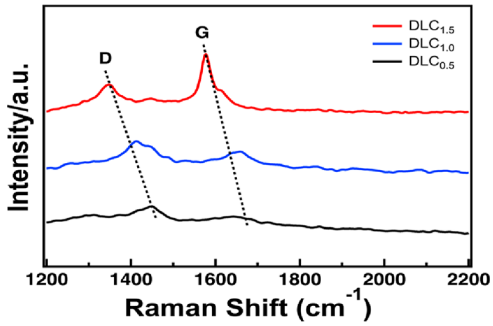

Figure 5. Raman spectra of $DLC_{0.5}$, $DLC_{1.0}$, and $DLC_{1.5}$ patterns.

in the D and G peak position, which were attributed to the variation in the sp^2−sp^3 hybridization content. The characteristic D and G peak in the carbon sample correspond to the disorder or defects arising from the breathing mode of *k*-point phonons of A_{1g} symmetry due to the loss translation symmetry and stretching vibrational mode of the C−C sp^2-bonded ring or chain structures that give rise to the doubly degenerated E_{2g} modes at the Brillouin zone center. The DLC film obtained at high applied dc (i.e., $DLC_{1.5}$) resulted in a broad D and a sharp

https://doi.org/10.1021/acsomega.3c01322
ACS Omega 2023, 8, 17053−17063

G peak obtained at 1350 and 1580 cm^{-1}, respectively. The evolution of the prominent D band in the $DLC_{1.5}$ is attributed to containing a higher sp^3 component from the diamond phase in the DLC film.[35] The sharp G band in the spectrum resulted from the well-defined sp^2-bonded graphitic nature of the carbon nanomatrix.[36] The broader D and G bands were centered at around 1450−1430 and 1655−1650 cm^{-1} in both $DLC_{0.5}$ and $DLC_{1.0}$ films, respectively. The upward shift in the D band Raman signal may attribute to the distorted and stress-induced C−C bonding formation in the carbon structures at the lower rate of decomposition of the ethanol solvent.[35,37,38] In this submerged plasma-based decomposition, slower rate decomposition of organic solvents may result in a hydrogenated amorphous carbon (a-C:H)-type thin film. Hydrogenation in the carbon structures usually tampered the C−C bonding angle and length. This resulted in a longer phonon interaction due to the presence of larger bonding of C−CH molecules. Again, from Guo et al.,[39,40] the pulse-modulated DLC deposition from various organic solvents showed the broadened D and G band under low dc bias conditions of DLC patterns, which may attribute to the small granular carbon deposits as well as the high amount of hydrogen content. The decreasing trends in the intensity ratio of the D band to the G band, i.e., I_D/I_G were found to be 1.14, 1.10, and 0.66 in $DLC_{0.5}$, $DLC_{1.0}$, and $DLC_{1.5}$, respectively, were attributed to the increasing order in the sp^3 content in the DLC patterns.[3,5,6,41] The lowest I_D/I_G in the $DLC_{1.5}$ patterned film indicates a high sp^3−sp^2 ratio in the DLC film as compared to $DLC_{0.5}$ and $DLC_{1.0}$.

The quantification of chemical composition and functional bonding in the as-synthesized DLC thin film patterns has been carried out by XPS spectral analysis. The survey spectrum with a high resolution C 1s spectrum (inset) of the $DLC_{1.5}$ film is shown in Figure 6. The C 1s spectrum of each DLC film has

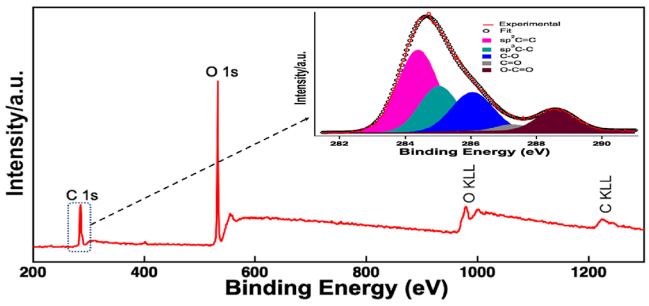

Figure 6. Survey scan of XPS (inset: high-resolution XPS C 1s) of the $DLC_{1.5}$ patterned film.

been deconvoluted into five peaks corresponding to carbon bonding and functionalization. The peaks centered at around 284.5, 285.2, 286.5, 287.1, and 288.5 eV in all the three types of DLC films correspond to the C═C (sp^2-hybridized carbon atoms), C−C (sp^3-hybridized carbon atoms), C−O (hydroxyl/ether), C═O (carbonyl), and O—C═O (carboxyl) bonds, respectively.[42,43] The evolution of oxidation reaction at the anodic silicon substrate occurs while depositing carbon radicals. The chemical bonding between carbon atoms and their native functionalization on the surface of the DLC films was quantified (as shown in Table 2) from the high-resolution C 1s spectra. By increasing the applied bias, the sp^3 contents (sp^3−sp^2 ratio) in the DLC film increase, as shown in Table 2. In the $DLC_{1.5}$ film, the sp^3−sp^2 ratio is 0.52 as compared to

Table 2. Parameters of Carbon Bonding Quantification from the XPS C 1s Spectra of DLC Films

	types of bonding (at %)					
type of DLC film	sp^2 C═C	sp^3 C−C	C−O	C═O	O—C═O	
$DLC_{0.5}$	48.4	16.2	18.8	5.5	10.9	0.33
$DLC_{1.0}$	51.9	20.1	14.4	1.4	12.2	0.39
$DLC_{1.5}$	43.7	22.6	20.8	2.5	10.4	0.52

0.33 and 0.39 in $DLC_{0.5}$ and $DLC_{1.0}$ films, respectively. These results depict the linear increase in hardness (sp^3 bonding) contents in the DLC films synthesized with a higher applied dc bias.[40] The XPS spectra of $DLC_{0.5}$ and $DLC_{1.0}$ patterned films are given in the Supporting Information, Figure S6.

4.4. Mechanism. The continuous microplasma state at the ultrasharp W-tip surface has been achieved by applying very strong cathodic dc biases of 0.5, 1.0, and 1.5 kV. As a result, a very highly dense micron-sized ionized state in the solvent (ethanol) medium was produced by the W-probe due to the emission of high electron density flux.[27,28] The microplasma-induced radical entities such as proton (H^+), electron (e^-), hydroxyl anion (OH^-), and various carbon radicals (C*, C_2^-, C_2H^-, $C_2H_2^+$, and $C_2H_3^+$) are microchanneling toward the anodized silicon substrate. The carbon patterns of the thin film are fabricated by the bottom-up approach, where the carbon radicals/molecules were assembled onto the silicon surface within a few seconds of applying the dc bias to the solvent-immersed W-tip. With the applied highly concentric energetic electron flux from the sharpen W-tip into the ethanol solvent, it dissociated into various ions and radicals.[31,44,45] In this anodic deposition process, the possible breakdown of the bonds and ionization of ethanol molecules may include the (i) $C_2H_5O^{\delta-}$, (ii) ethyl ($C_2H_5^*$), (iii) methyl (CH_3^*), (iv) methylene (CH_2^-), and (v) hydroxyl (OH^-) groups, which play a vital role in the formation of the carbon hybrid thin film with different hydro-oxygenation functionalizations onto the substrate. A schematic of the fabrication process is given in Figure 7a, depicting a schematic experimental setup, the plasma discharge thermal flux from the submerged W-tip, decomposition of the hydrocarbon source, and subsequent DLC fabrication on the silicon surface in the pure ethanol solvent. The decomposed carbon radicals were deposited onto the anodized silicon substrate with varying sp^2 and sp^3 hybridization contents. It is because during the DLC deposition, the current was maintained at a constant of 1 mA, and the distance between the cathode and anode has varied at ca. 0.825 μm each time rising to 500 V. Therefore, with increasing the dc bias, the ethanol quantity beneath the cathodic W-tip has also been increased. This in turn favors the decomposition and increases the patterning of RoD. A schematic overview of change in the overall morphologies, surface functionalization, grain boundaries of carbon deposit, and RoD variation is given in Figure 7b. At low dc bias, i.e., $DLC_{0.5}$, the cathodic W-tip was ca. 1 mm apart from the anode silicon substrate. The decomposition of ethanol in the influence of the plasmonic W-tip is occurs in a very narrow channel. In this case, small grain sizes of carbon deposit with higher roughness from SEM and AFM analysis have been observed. Under $DLC_{1.0}$ conditions, the distance between the cathode and anode has increased, with a wide ethanol channel. This induces a growth phase of the DLC deposit with high RoD. Again, under $DLC_{1.5}$ conditions, the ethanol channel is

https://doi.org/10.1021/acsomega.3c01322
ACS Omega 2023, 8, 17053−17063

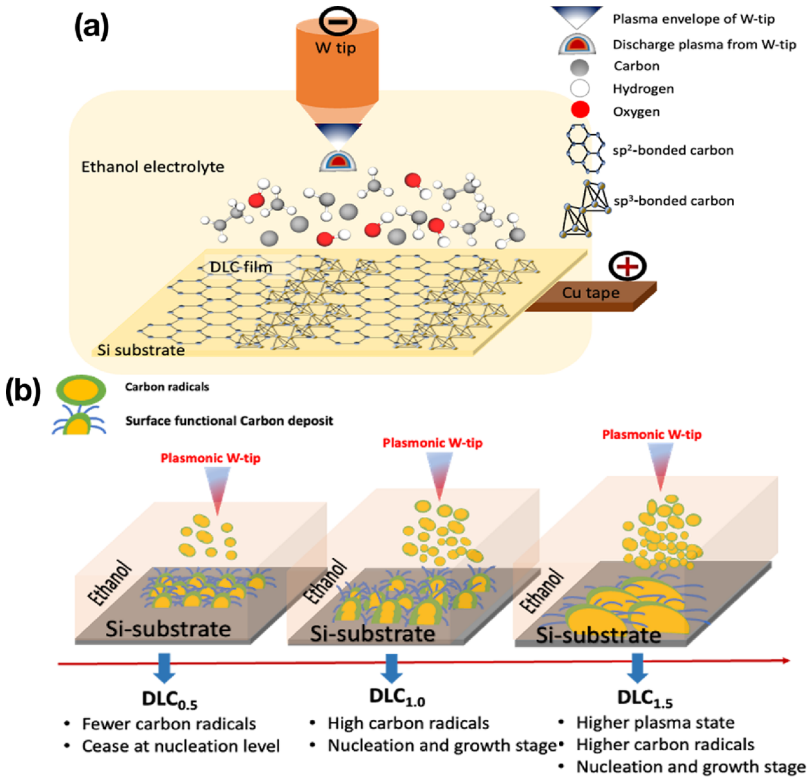

Figure 7. Schematic showing the plasma discharge from the sharpen W-tip and DLC patterning mechanism (a) and the experimental DLC pattern formation (b) onto the silicon substrate.

Table 3. Energy Consumption of the DLC Coating Film by Various Methods

techniques	PVD[a]	CVD[a]	electrochemistry	SSP (this work)
approximate energy consumption(in kWh)	$\sim 10^2$ order	$\sim 10^3$ order	$\sim 10^{-7}$ to 10^2	2.25×10^{-4}(for $DLC_{1.5}$)
subsequent steps for patterning	masking	etching	high temperature	direct pattern formation without any further additional steps
	etching	cooling	masking	
	annealing	fabrications	etching	

[a]Only our SSP includes pattern formation. Approximate energy consumption shown here deals with other (not DLC) coating materials.

wider for voluminous ethanol decomposition and deposition onto the silicon substrate. From the above physicochemical analysis of DLC samples, the $DLC_{1.5}$ has shown a smoother surface, low grain boundaries, and high sp^3 diamond phase in the carbon matrix.

4.5. Soft Solution Process: Lowest Consumption Energy. Material processing, in general, has multiple steps but follows a two-step process, i.e., (i) chemical synthesis and then (ii) fabrication process into size and shape-fixed-like desired patterns, for various applications. Today's various advanced material processing techniques such as PVD and CVD were consuming huge amounts of energies throughout the entire end-user fabrication stage. These include (i) multistep masking and etching, (ii) heating/annealing, and (iii) vacuum or artificial atmosphere requirements during the entire process. In brief, high consumption of energies, release of toxic gases, release of waste materials, and heat to the environments are of great concern toward the sustainable material processing techniques. In 2000, Yoshimura, one of the authors, has proposed various "soft solution processing (SSP)" techniques[25] as a novel strategy for synthesis and fabrication at the expense of the lowest possible energies. This reveals that the driving forces required for the synthesis of an inorganic material (for example $BaTiO_3$) from (i) solid to solid, (ii) gas(es) to solid, (iii) gas(es) and ions to solid, (iv) (solid + liquid) to solid, and (v) liquid to solid consume energies of 38, 727, 3685, 17, and −14 kcal/mol, respectively, at room temperature. This study depicts the material processing/fabrication in the solution phase, which involve the significant reduction in the energy consumption. For sustainability, we must consider the material processing staring from the solution phase and to understand the complex material formation mechanisms. Herewith, the approximate overall energy consumption by various material processing techniques is given in Table 3. Although, it is impractical to calculate the exact values of energies since they significantly vary with the machinery operating process parameters, nature and size of fabricated materials, and pre-/post-processing (annealing, cooling, cleaning, etc.) steps. A typical case study[46] of the total energy consumption shows that thin film hard coatings of TiN and TiCN (not to be confused with "patterns") by PVD and CVD were 112 and 974 kWh, respectively. In a similar approach, conventional electrochemical techniques (including electrochemical deposition, electrophoretic deposition, and pulse electrochemical deposition)[44,47−51] utilize very low energies but require many further processing techniques such as high temperature to consolidation, moreover making patterns and other expensive processing like masking, etching,

https://doi.org/10.1021/acsomega.3c01322
ACS Omega 2023, 8, 17053−17063

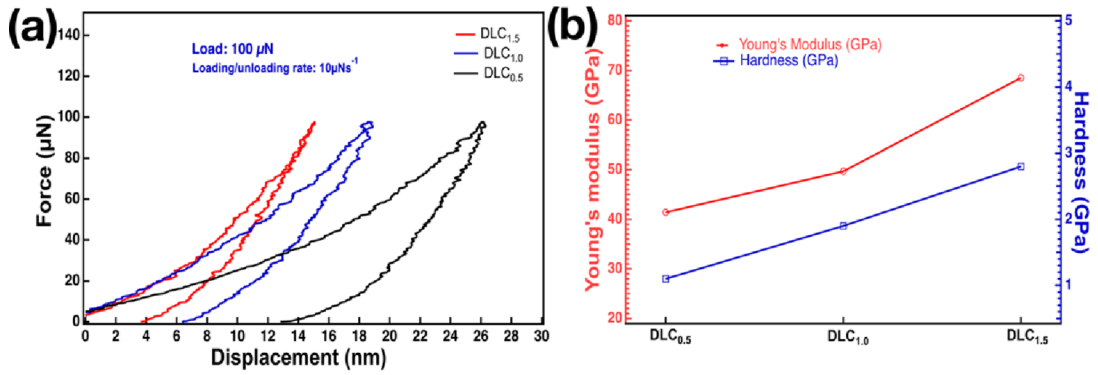

Figure 8. Load-displacement curves (a) and Young's modulus and hardness plot (b) of $DLC_{0.5}$, $DLC_{1.0}$, and $DLC_{1.5}$.

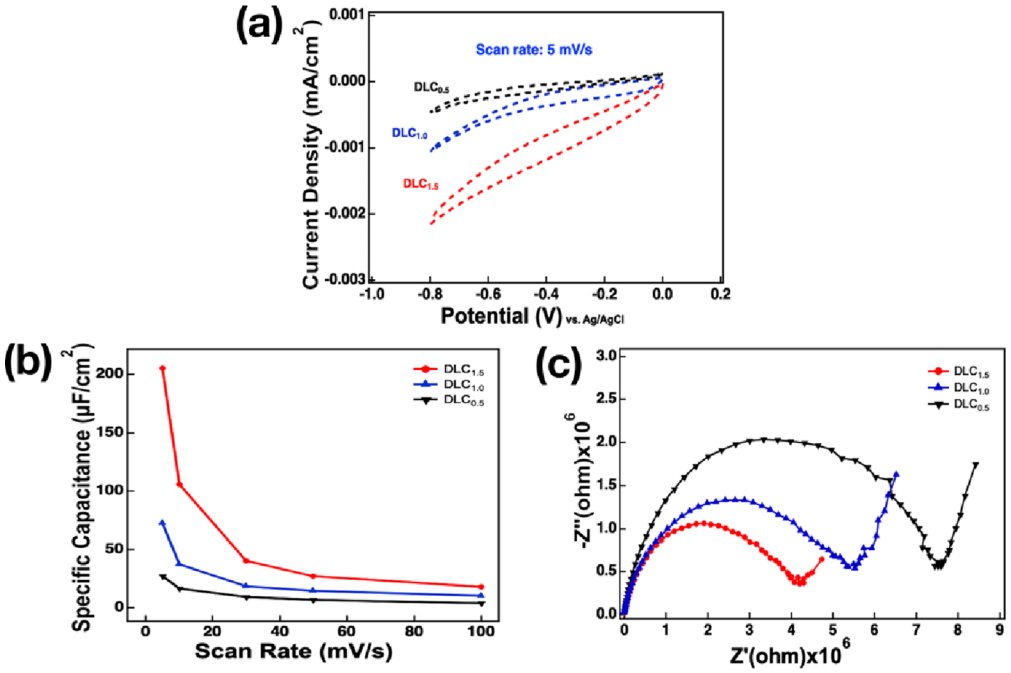

Figure 9. Cyclic voltammetry of $DLC_{0.5}$, $DLC_{1.0}$, and $DLC_{1.5}$ of a scan rate of 5 mV/s (a), specific capacitances vs current density (b), and impedance spectra (c) of DLC electrodes.

etc. In contrast to all the other mentioned techniques, the proposed SSP technique can prepare the DLC or any other novel materials (inorganics) directly onto the conducting substrate as pattern(s). Therefore, we would like to appeal herewith that "direct patterning of DLC" is possible in simple equipment under ambient conditions, thus with the lowest energy consumption, and minimizes wastes and harmful byproducts, even though our products are in the primitive stage of innovation.

4.6. Mechanical Properties of the DLC Patterned Films. Nanoindentation measurements were performed to the as-synthesized DLC patterned films to measure the elastic modulus and hardness properties. The test was performed by a Berkovich geometry of a diamond tip with an applied load of 100 μN at a loading and unloading rate of 10 μN/s. The force-displacement plot from Figure 8a shows the intriguing mechanical character of the DLC patterned films prepared under various dc bias applied conditions. The lowest displacement up to 15 nm has been observed in $DLC_{1.5}$ that may attribute to the higher sp^3 phase in the carbon structures. The displacements have been increased to 18.7 and 26 nm in $DLC_{1.0}$ and $DLC_{0.5}$, respectively, showing the softness of the DLC films at lower applied dc bias. The measured value of Young's modulus and hardness values are assessed from the TriboScan software analysis and interpreted in plotting Figure 8b. Young's moduli show 41.4, 49.7, and 68.5 GPa for the $DLC_{0.5}$, $DLC_{1.0}$, and $DLC_{1.5}$, respectively. The hardness values show 1.1, 1.9, and 2.8 GPa for $DLC_{0.5}$, $DLC_{1.0}$, and $DLC_{1.5}$, respectively. The increasing trend in Young's modulus and hardness is attributed to the increasing order of the sp^3 phase (diamond phase) in the DLC patterns. However, since the DLC patterns were made from the hydrocarbon source (ethanol), hydrogenation in the carbon structures is the dominant factor for their softness and results in comparable mechanical strengths as reported in other studies.[52−57]

4.7. Electrochemical Analysis of the DLC Patterned Films. DLC is a well-studied electrode material due to its large potential window and chemical stability.[58] As-fabricated DLC patterns were explored for the electrochemical charge storage mechanism in a neutral electrolyte of 0.5 M Na_2SO_4. Figure S7a−c shows the cyclic voltammetry analysis of $DLC_{0.5}$, $DLC_{1.0}$, and $DLC_{1.5}$ pattern electrodes at 5−100 mV/s scan

https://doi.org/10.1021/acsomega.3c01322
ACS Omega 2023, 8, 17053−17063

rates, respectively. The shape of the CV curve changes from a shallow to a deep quasi-rectangular form, which may be attributed to the increase in pseudo-capacitive behavior in the DLC films. In lower to higher dc bias pattern structures, the grain sizes were increased, as observed by SEM images. This in turn may increase the grain boundary and hence the surface resistance.[59] At lower scan rate, the measured specific capacitance (eq 1) is shown to be maximum for the DLC samples. For comparison, CV of all the prepared carbon electrodes at 5 mV/s scan rate is given in Figure 9a. The specific capacitances of $DLC_{0.5}$, $DLC_{1.0}$, and $DLC_{1.5}$ carbon electrodes at 5 mV/s are 27, 72, and 205 $\mu F/cm^2$, respectively. The shape of the CV curves that widen from $DLC_{0.5}$ to $DLC_{1.5}$ was due to the structural changes in the DLC film, which presume development of more conductive sites for the charge storage.[60] The variation in the capacitance of the as-prepared DLC electrodes with respect to the scan rates is given in Figure 9b. The measured specific capacitances of the $DLC_{0.5}$ pattern at 5, 10, 30, 50, and 100 mV/s scan rates are 27, 16.8, 9.2, 6.9, and 4.1 $\mu F/cm^2$, respectively. For the $DLC_{1.0}$ pattern, the measured specific capacitances at 5, 10, 30, 50, and 100 mV/s scan rates were 72.3, 37.1, 18.7, 14.6, and 10.3 $\mu F/cm^2$, respectively. For the $DLC_{1.5}$ pattern, the measured specific capacitances at 5, 10, 30, 50, and 100 mV/s scan rates were 205, 105.9, 40.4, 27.4, and 18.3 $\mu F/cm^2$, respectively. The electrochemical resistance at the electrolyte−electrode interface has been measured from the electrochemical impedance spectroscopy (EIS) analysis. The EIS analysis, as shown in Figure 9c, reveals the high resistive nature of all the three conditioned DLC electrodes (i.e., $DLC_{0.5}$, $DLC_{1.0}$, and $DLC_{1.5}$), which is attributed to their amorphous and non-conductive nature. The $DLC_{0.5}$ carbon electrode showed the highest R_{ct} value, which can be measured from the diameter of a semicircle. The $DLC_{1.5}$ carbon electrode showed the smallest R_{ct} value, indicating higher conductivity than $DLC_{0.5}$ and $DLC_{1.0}$, as shown in Figure 9c. $DLC_{0.5}$, $DLC_{1.0}$, and $DLC_{1.5}$ carbon R_{ct} values are 7.68×10^6, 5.63×10^6, and 4.37×10^6 Ω, respectively. The EIS spectra of all types of the DLC pattern show relative higher resistance at the solid (DLC)−electrolyte interface due to the non-conductive sp^3 phase contents.[61]

5. CONCLUDING REMARKS AND PERSPECTIVE

In this report, we have succeeded in preparing DLC patterns on the silicon substrate under ambient conditions by a process using copious amounts of solvent (∼4 to 5 mL) and that is fast (within 10 min), green (lowest consumption of energies), and sustainable for the first time. The submerged conditioned microplasma-based electrochemical approach in preparing carbon nanostructures from a simple solvent (in this case, ethanol) may show profound interest to the science community. The present work describes the evolution of DLC pattern formation in the submerged state assisted with plasma and electrochemical driving forces. The plasma-based decomposition of absolute ethanol into various carbonaceous polar molecules is micro-channelized toward the substrate and subsequently patterned. However, this simple and quick step of patterning of DLC onto the silicon substrate involves complex phenomena, such as (i) high temperature gradient between the W-tip and Si substrate in the submerged state of reaction, (ii) electrophoretic force between anodized silicon and polar carbon molecules/ions/radicals at high applied dc bias, and (iii) *in situ* decomposition of ethanol and their nature of hybridizations (sp^3, sp^2, and sp) while deposited onto the substrate. The complete understanding of the above-mentioned mechanism required further efforts to detailed analysis and beyond the scope of this first proposed research article. However, from the detailed studies performed, DLC patterns are well concluded. Under higher applied dc bias conditions, the rate of deposition has been significantly enhanced; as a result, the large area uniform distributions, decrease in surface roughness, and increase in grain sizes in the carbon structures have been obtained. From the spectroscopy analysis, the nature of surface functionalizations, types of hybridizations, and their quantifications have been accessed. Endowment of hydrogen and oxygen functional groups on the patterned DLC structures has been confirmed from FTIR spectra. From Raman spectral analysis, the mixed phases of sp^3 (diamond phase) and sp^2 (graphitic phase) have been confirmed from the existing D and G band shift, respectively. The lowest I_D/I_G ratio in the DLC pattern at higher dc bias shows a high sp^3−sp^2 ratio. The XPS analysis provides the quantified carbon functionalization in the DLC structures and shows the increase in sp^3 (diamond phase) with an increase in the applied dc bias. Furthermore, the mechanical behavior has been assessed by nanoindentation studies. The increase in Young's modulus and hardness with the increase in applied dc bias is attributed to the rise of the sp^3 phase in the patterned DLC. From the electrochemical studies, the higher specific capacitance for $DLC_{1.5}$ was noted due to the fully formed DLC film as compared to the $DLC_{0.5}$ and $DLC_{1.0}$.

In perspective, the lowest energy consumption in formation to the DLC pattern in one step under ambient conditions of temperature and pressure within a very short period is unique. However, complete understanding of the favorable reaction mechanism is very complex and requires more efforts and further explorations. Since the process technique uses the lowest energy in forming DLC patterns, the significance in their further exploration is very important in terms of "green and sustainable" production technologies. The proposed simple and economically favored soft solution process may pave the way for further consideration of functional DLC patterning effectively.

■ ASSOCIATED CONTENT

Supporting Information

The Supporting Information is available free of charge at https://pubs.acs.org/doi/10.1021/acsomega.3c01322.

Fabrication process of the W-tip, SEM image of the W-tip, mathematical thermal emissive model of the W-tip, rate of deposition studies by surface profilometry data analysis, three-dimensional AFM images, SEM images, XPS spectra, and cyclic voltammetry studies of DLC patterns (PDF)

■ AUTHOR INFORMATION

Corresponding Author

Masahiro Yoshimura − *Department of Materials Science and Engineering, National Cheng Kung University, Tainan 70101, Taiwan;* orcid.org/0000-0003-1810-0301; Phone: +886-6-2757575; Email: yoshimur@ncku.edu.tw

Authors

Sumanta Kumar Sahoo − *Department of Materials Science and Engineering, National Cheng Kung University, Tainan 70101, Taiwan;* orcid.org/0000-0002-4625-3412

https://doi.org/10.1021/acsomega.3c01322
ACS Omega 2023, 8, 17053−17063

Ravi Bolagam − *Department of Materials Science and Engineering, National Cheng Kung University, Tainan 70101, Taiwan*
Kripasindhu Sardar − *Department of Materials Science and Engineering, National Cheng Kung University, Tainan 70101, Taiwan*
Satoru Kaneko − *Department of Materials Science and Engineering, National Cheng Kung University, Tainan 70101, Taiwan; Kanagawa Institute of Industrial Science and Technology, Ebina, Kanagawa 243-0435, Japan*
Shih-Chen Shi − *Department of Mechanical Engineering, National Cheng Kung University, Tainan 70101, Taiwan*
Kao-Shuo Chang − *Department of Materials Science and Engineering, National Cheng Kung University, Tainan 70101, Taiwan;* orcid.org/0000-0002-2876-9255

Complete contact information is available at: https://pubs.acs.org/10.1021/acsomega.3c01322

Notes

The authors declare no competing financial interest.

■ ACKNOWLEDGMENTS

Authors S.K.S., R.B., S.K., and M.Y. would like to thank the NCKU: 90 & Beyond programme (grant no. D110-G2309), and Amanda foundation under contract no. AF-2020227-B3 for the financial support to carry out the research work. The authors S.K.S. and S.K. are thankful to Dr. Yasuhiro Naganuma, KISTECH, Japan for helping in chemical analysis to the DLC patterns.

■ REFERENCES

(1) Yang, N.; Jiang, X. Rational design of diamond electrodes. *Acc. Chem. Res.* **2023**, *56*, 117−127.
(2) Robertson, J. Diamond-like amorphous carbon. *Mater. Sci. Eng.: R: Reports* **2002**, *37*, 129−281.
(3) Wang, Y.; Zhang, M.; Wang, Y.; Zhang, G.; Lu, Z. Influence of currents on tribological behavior of diamond-like carbon films. *Appl. Phys. A: Mater. Sci. Process.* **2020**, *126*, 1−11.
(4) Salinas Ruiz, V. R.; Kuwahara, T.; Galipaud, J.; Masenelli-Varlot, K.; Ben Hassine, M.; Héau, C.; Stoll, M.; Mayrhofer, L.; Moras, G.; Martin, J. M.; Moseler, M.; de Barros Bouchet, M.-I. Interplay of mechanics and chemistry governs wear of diamond-like carbon coatings interacting with ZDDP-additivated lubricants. *Nat. Commun.* **2021**, *12*, 4550.
(5) Kabir, M. S.; Zhou, Z.; Xie, Z.; Munroe, P. Designing multilayer diamond like carbon coatings for improved mechanical properties. *J. Mater. Sci. Technol.* **2021**, *65*, 108−117.
(6) Luo, B.; Yuan, A.; Yang, S.; Han, L.; Guan, R.; Duan, J.; Wang, C.; Dong, L.; Zhang, B.; Li, D. Synthesis of diamond-like carbon as a dielectric platform for graphene field effect transistors. *ACS Appl Nano Mater* **2021**, *4*, 1385−1393.
(7) Nistor, P. A.; May, P. W. Diamond thin films: giving biomedical applications a new shine. *J. R. Soc., Interface* **2017**, *14*, 20170382.
(8) Aisenberg, S.; Chabot, R. Ion-beam deposition of thin films of diamondlike carbon. *J. Appl. Phys.* **1971**, *42*, 2953−2958.
(9) Plotnikov, V. A.; Demyanov, B. F.; Makarov, S. V. Atomic structure of carbon clusters laser-produced diamond-like carbon films. *Diamond Relat. Mater.* **2021**, *114*, No. 108334.
(10) Anders, A.; Fong, W.; Kulkarni, A. V.; Ryan, F. W.; Bhatia, C. S. Ultrathin diamond-like carbon films deposited by filtered carbon vacuum arcs. *IEEE Trans. Plasma Sci.* **2001**, *29*, 768−775.
(11) Ruoff, R. S.; Lee, K. H.; Lee, S. H. Synthesis of diamond-like carbon nanofiber films. *ACS Nano* **2020**, *14*, 13663−13672.
(12) Iwamoto, Y.; Hirata, Y.; Takamura, R.; Akasaka, H.; Ohtake, N. Deposition phenomena of diamond-like carbon coating on inner surface of circular metal tube by nanopulse plasma chemical vapor deposition. *Diamond Relat. Mater.* **2022**, *121*, No. 108749.
(13) Lou, Z.; Chen, Q.; Zhang, Y.; Wang, W.; Qian, Y. Diamond formation by reduction of carbon dioxide at low temperatures. *J. Am. Chem. Soc.* **2003**, *125*, 9302−9303.
(14) Liang, C.; Chen, Y.; Wu, M.; Wang, K.; Zhang, W.; Gan, Y.; Huang, H.; Chen, J.; Xia, Y.; Zhang, J.; Zheng, S.; Pan, H. Green synthesis of graphite from CO_2 without graphitization process of amorphous carbon. *Nat. Commun.* **2021**, *12*, 119.
(15) Watanabe, T.; Ohba, T. Low-temperature CO_2 thermal reduction to graphitic and diamond-like carbons using perovskite-type titanium nanoceramics by quasi-high-pressure reactions. *ACS Sustainable Chem. Eng.* **2021**, *9*, 3860−3873.
(16) May, P. W. Diamond thin films: A 21st-century material. *Philosophical Transactions of the Royal Society of London. Series A: Mathematical, Physical and Engineering Sciences* **2000**, *358*, 473−495.
(17) Namba, Y. Attempt to grow diamond phase carbon films from an organic solution. *J. Vac. Sci. Technol., A* **1992**, *10*, 3368−3370.
(18) Fu, Q.; Jiu, J.-T.; Cao, C.-B.; Wang, H.; Zhu, H.-S. Electrodeposition of carbon films from various organic liquids. *Surf. Coat. Technol.* **2000**, *124*, 196−200.
(19) Suzuki, T.; Manita, Y.; Yamazaki, T.; Wada, S.; Noma, T. Deposition of carbon films by electrolysis of a water-ethylene glycol solution. *J. Mater. Sci.* **1995**, *30*, 2067−2069.
(20) Jiang, H.; Huang, L.; Wang, S.; Zhang, Z.; Xu, T.; Liu, W. Synthesis of DLC films by electrolysis of dimethyl sulfoxide. *Electrochem. Solid-State Lett.* **2004**, *7*, D19−D21.
(21) Cai, K.; Guo, D.; Huang, Y.; Zhu, H.-S. Evaluation of diamond-like carbon films deposited on conductive glass from organic liquids using pulsed current. *Surf. Coat. Technol.* **2000**, *130*, 266−273.
(22) Novikov, V. P.; Dymont, V. P. Mechanism for electrochemical synthesis of diamond-like carbon. *Tech. Phys. Lett.* **1997**, *23*, 350−351.
(23) Yoshimura, M. Importance of soft solution processing for advanced inorganic materials. *J. Mater. Res.* **1998**, *13*, 796−802.
(24) Yoshimura, M.; Livage, J. Soft processing for advanced inorganic materials. *MRS Bull.* **2000**, *25*, 12−13.
(25) Yoshimura, M.; Suchanek, W. L.; Byrappa, K. Soft solution processing: a strategy for one-step processing of advanced inorganic materials. *MRS Bull.* **2000**, *25*, 17−25.
(26) Watanabe, T.; Wang, H.; Yamakawa, Y.; Yoshimura, M. Direct carbon patterning on a conducting substrate in an organic liquid. *Carbon* **2006**, *44*, 799−801.
(27) Chokradjaroen, C.; Wang, X.; Niu, J.; Fan, T.; Saito, N. Fundamentals of solution plasma for advanced materials synthesis. *Mater Today Adv.* **2022**, *14*, No. 100244.
(28) Saito, N.; Bratescu, M. A.; Hashimi, K. Solution plasma: a new reaction field for nanomaterials synthesis. *Jpn. J. Appl. Phys.* **2018**, *57*, No. 0102A4.
(29) Ghadai, R. K.; Das, S.; Kalita, K.; Swain, B. P.; Davim, J. P. Structural and mechanical analysis of APCVD deposited diamond-Like carbon thin films. *Silicon* **2021**, *13*, 4453−4462.
(30) Swain, B. P. The analysis of carbon bonding environment in HWCVD deposited A-SiC:H films by XPS and raman spectroscopy. *Surf. Coat. Technol.* **2006**, *201*, 1589−1593.
(31) Li, Y.; Zhang, G.; Hou, X.; Deng, D. Growth mechanism of carbon films from organic electrolytes. *J. Mater. Sci.* **2013**, *48*, 3505−3510.
(32) Fu, Y.; Zhang, J.; Liu, H.; Hiscox, W. C.; Gu, Y. Ionic liquid-assisted exfoliation of graphite oxide for simultaneous reduction and functionalization to graphenes with improved properties. *J. Mater. Chem. A* **2013**, *1*, 2663.
(33) Kumar, N. A.; Choi, H.-J.; Shin, Y. R.; Chang, D. W.; Dai, L.; Baek, J.-B. Polyaniline-grafted reduced graphene oxide for efficient electrochemical supercapacitors. *ACS Nano* **2012**, *6*, 1715−1723.
(34) Abdolmaleki, A.; Mallakpour, S.; Borandeh, S. Improving interfacial interaction of L-phenylalanine-functionalized graphene nanofiller and poly(vinyl alcohol) nanocomposites for obtaining significant membrane properties: morphology, thermal, and mechanical studies. *Polym. Compos.* **2016**, *37*, 1924−1935.

(35) Zhao, F.; Afandi, A.; Jackman, R. B. Graphene diamond-like carbon films heterostructure. *Appl. Phys. Lett.* **2015**, *106*, No. 102108.
(36) Lan, G.; Qiu, Y.; Fan, J.; Wang, X.; Tang, H.; Han, W.; Liu, H.; Liu, H.; Song, S.; Li, Y. Defective graphene@diamond hybrid nanocarbon material as an effective and stable metal-free catalyst for acetylene hydrochlorination. *Chem. Commun.* **2019**, *55*, 1430−1433.
(37) Yan, X.; Xu, T.; Chen, G.; Xue, Q. J.; Yang, S. R. Synthesis of diamond-like carbon/nanosilica composite films by an electrochemical method. *Electrochem. Commun.* **2004**, *6*, 1159−1162.
(38) Huang, L.; Jiang, H.; Zhang, J.; Zhang, Z.; Zhang, P. Synthesis of copper nanoparticles containing diamond-like carbon films by electrochemical method. *Electrochem. Commun.* **2006**, *8*, 262−266.
(39) Guo, D.; Cai, K.; Li, L.; Zhu, H. Preparation of hydrogenated diamond-like carbon films on conductive glass from an organic liquid using pulsed power. *Chem. Phys. Lett.* **2000**, *325*, 499−502.
(40) Guo, D.; Cai, K.; Li, L.; Huang, Y.; Gui, Z.; Zhu, H. Evaluation of diamond-like carbon films electrodeposited on an Al substrate from the liquid phase with pulse-modulated power. *Carbon* **2001**, *39*, 1395−1398.
(41) Chen, J.; Ji, P.; Jin, C.; Zhuge, L.; Wu, X. The properties of N-doped diamond-like carbon films prepared by helicon wave plasma chemical vapor deposition. *Plasma Science and Technology* **2019**, *21*, No. 025502.
(42) Wongpanya, P.; Silawong, P.; Photongkam, P. Adhesion and corrosion of Al−N doped diamond-like carbon films synthesized by filtered cathodic vacuum arc deposition. *Ceram. Int.* **2022**, *48*, 20743−20759.
(43) Elam, F. M.; Hsia, F.-C.; van Vliet, S.; Bliem, R.; Yang, L.; Weber, B.; Franklin, S. E. The influence of corrosion on diamond-like carbon topography and friction at the nanoscale. *Carbon* **2021**, *179*, 590−599.
(44) Li, Y.; Zhang, G.; Hou, X.; Deng, D. Synthesis and tribological properties of diamond-like carbon films by electrochemical anode deposition. *Appl. Surf. Sci.* **2012**, *258*, 6527−6530.
(45) Li, Y.; Zhang, G.-F.; He, Y.-Y.; Hou, X.-D. Electrical double layer model and thermodynamic coupling for electrochemically deposited hydrogenated amorphous carbon films. *J. Electrochem. Soc.* **2012**, *159*, H918−H920.
(46) Gassner, M.; Rebelo de Figueiredo, M.; Schalk, N.; Franz, R.; Weiß, C.; Rudigier, H.; Holzschuh, H.; Bürgin, W.; Pohler, M.; Czettl, C.; Mitterer, C. Energy consumption and material fluxes in hard coating deposition processes. *Surf. Coat. Technol.* **2016**, *299*, 49−55.
(47) Tsukada, J.; Zanin, H.; Barbosa, L. C. A.; da Silva, G. A.; Ceragioli, H. J.; Peterlevitz, A. C.; Teófilo, R. F.; Baranauskas, V. Electro-deposition of carbon structures at mid voltage and room temperature using ethanol/aqueous solutions. *J. Electrochem. Soc.* **2012**, *159*, D159−D161.
(48) Shevchenko, E.; Matiushenkov, E.; Kochubey, D.; Sviridov, D.; Kokorin, A.; Kulak, A. Synthesis of carbon films with diamond-like structure by electrochemical oxidation of lithium acetylide. *Chem. Commun.* **2001**, *4*, 317−318.
(49) Mayama, N.; Yoshida, H.; Iwata, T.; Sasakawa, K.; Suzuki, A.; Hanaoka, Y.; Morita, Y.; Kuroda, A.; Owari, M. Characterization of carbonaceous films deposited on metal substrates by liquid-phase electrodeposition in methanol. *Diamond Relat. Mater.* **2010**, *19*, 946−949.
(50) Sreejith, K.; Nuwad, J.; Pillai, C. G. S. Low voltage electrodeposition of diamond like carbon (DLC). *Appl. Surf. Sci.* **2005**, *252*, 296−302.
(51) Wang, H.; Shen, M.-R.; Ning, Z.-Y.; Ye, C.; Zhu, H.-S. Pulsed electrodeposition of diamond-like carbon films. *J. Mater. Res.* **1997**, *12*, 3102−3105.
(52) Ghadai, R. K.; Das, S.; Kalita, K.; Shivakoti, I.; Mondal, S. C.; Swain, B. P. Effect of nitrogen (N2) flow rate over the tribological, structural and mechanical properties diamond-like carbon (DLC) thin film. *Mater. Chem. Phys.* **2021**, *260*, No. 124082.
(53) Xu, Y.; Jia, J.; Zhang, G.; Li, H.; Chen, T. Effect of rubber substrates on the flexibility and tribological properties of diamond-like carbon coatings. *Surf. Coat. Technol.* **2021**, *422*, No. 127526.
(54) Su, Y.; Huang, W.; Cai, L.; Gong, X.; Zhang, T.; Hu, R.; Zhang, P.; Ruan, H. Microstructural evolution and tribology of Mo-doped diamond like carbon nanocomposite film. *Tribol Int* **2022**, *174*, No. 107774.
(55) Wang, X.; Zhang, X.; Wang, C.; Lu, Y.; Hao, J. High temperature tribology behavior of silicon and nitrogen doped hydrogenated diamond-like carbon (DLC) coatings. *Tribol Int* **2022**, *175*, No. 107845.
(56) Liu, M.; Yan, F. Scratch-induced deformation and damage behavior of doped diamond-like carbon films under progressive normal load of vickers indenter. *Thin Solid Films* **2022**, *756*, No. 139351.
(57) Wang, M.; Zhang, L.; Lin, G. Improved mechanical and tribological properties of diamond-like carbon films by adjusting pulsed substrate bias. *Diamond Relat. Mater.* **2022**, *130*, No. 109402.
(58) Zeng, A.; Neto, V. F.; Gracio, J. J.; Fan, Q. H. Diamond-like carbon (DLC) films as electrochemical electrodes. *Diamond Relat. Mater.* **2014**, *43*, 12−22.
(59) Rachedi, N.; Hadjersi, T.; Moulai, F.; Dokhane, N.; Manseri, A.; Bouanik, S. Effect of electrolyte type on properties of diamond - like carbon films electrodeposited onto N-type Si substrate, application as electrode for supercapacitors. *Silicon* **2020**, *12*, 2445−2453.
(60) Kulak, A. I.; Kokorin, A. I.; Meissner, D.; Ralchenko, V. G.; Vlasov, I. I.; Kondratyuk, A.; Kulak, T. I. Electrodeposition of nanostructured diamond-like films by oxidation of lithium acetylide. *Electrochem. Commun.* **2003**, *5*, 301−305.
(61) Liu, E.; Kwek, H. W. Electrochemical performance of diamond-like carbon thin films. *Thin Solid Films* **2008**, *516*, 5201−5205.

https://doi.org/10.1021/acsomega.3c01322
ACS Omega 2023, 8, 17053−17063